avoid the additional matching networks and reduce the loading effect. Measured results reveal that the proposed circuit achieves a compact size, good passband response, and simple design, and all of these make the proposed four-channel diplexer attractive in wireless communication systems.

ACKNOWLEDGMENT

This work was supported in part by National Science Council, Taiwan, under contract no. MOST 103-2221-E-008-023.

REFERENCES

1. M.L. Chuang and M.T. Wu, Microstrip diplexer design using common T-shaped resonator, IEEE Microwave Wireless Compon Lett 21 (2011), 583–585.
2. C.F. Chen, T.Y. Huang, C.P. Chou, and R.B. Wu, Microstrip diplexers design with common resonator sections for compact size, but high isolation, IEEE Trans Microwave Theory Tech 54 (2006), 1945–1952.
3. P.H. Deng, M.I. Lai, S.K. Jeng, and C.H. Chen, Design of matching circuits for microstrip triplexers based on stepped-impedance resonators, IEEE Trans Microwave Theory Tech 54 (2006), 4185–4192.
4. C.F. Chen, T.M. Shen, T.Y. Huang, and R.B. Wu, Design of multimode net-type resonators and their applications to filters and multiplexers, IEEE Trans Microwave Theory Tech 59 (2011), 848–856.
5. J.Y. Wu, K.W. Hsu, Y.H. Tseng, and W.H. Tu, High-isolation microstrip triplexer using multiple-mode resonators, IEEE Microwave Wireless Compon Lett 22 (2012), 173–175.
6. C.F. Cheng, T.M. Shen, T.Y. Huang, and R.B. Wu, Design of compact quadruplexer based on the tri-mode net-type resonators, IEEE Microwave Wireless Compon Lett 21 (2011), 534–536.
7. S.J. Zeng, J.Y. Wu, and W.H. Tu, Compact and high-isolation quadruplexer using distributed coupling technique, IEEE Microwave Wireless Compon Lett 21 (2011), 197–199.
8. T.Y. Yun, C. Wang, P. Zepeda, C.T. Rodenbeck, M.R. Coutant, M.Y. Li, and K. Chang, A 10- to 21-GHz low-cost, multifrequency, and full-duplex phased-array antenna system, IEEE Trans Antennas Propag 50 (2002), 641–650.
9. S. Hong and K. Chang, A 10–35-GHz six-channel microstrip multiplexer for wide-band communication systems, IEEE Trans Microwave Theory Tech 54 (2006), 1370–1378.
10. B. Strassner and K. Chang, Wide-band low-loss high-isolation microstrip periodic-stub diplexer for multiple-frequency applications, IEEE Trans Microwave Theory Tech 49 (2001), 1818–1820.
11. Y. Ning, A new multiple-frequency millimeter diplexer using microstrip periodic-stub, In: IET International Conference on Wireless Mobile and Multimedia Networks Proceedings (ICWMMN 2006), Hangzhou, China, 2006, pp. 335–337.
12. H.W. Wu, S.H. Huang, and Y.F. Chen, Design of new quad-channel diplexer with compact circuit size, IEEE Microwave Wireless Compon Lett 23 (2013), 240–242.
13. D. Zayniyev and D. Budimir, Microstrip three-port 4-channel multiplexers using dual-band bandpass filters for wireless application, In: AP-S 2008. IEEE Antennas and Propagation Society International Symposium, San Diego, CA, 2008, pp. 1–4.
14. M.L. Lai and S.K. Jeng, A microstrip three-port and four-channel multiplexer for WLAN and UWB coexistence, IEEE Trans Microwave Theory Tech 53 (2005), 3244–3250.
15. M. Sagawa, M. Makimoto, and S. Yamashita, Geometrical structures and fundamental characteristics of microwave stepped-impedance resonators, IEEE Trans Microwave Theory Tech 45 (1997), 1078–1085.
16. J.S. Hong and M.J. Lancaster, Microstrip filters for RF/microwave applications, Wiley, New York, 2001.

DESIGN OF MICROSTRIP PATCH ANTENNAS WITH IMPROVED LOW-ELEVATION GAIN FOR CRPA APPLICATIONS

Sungjun Yoo,[1] Gangil Byun,[2] and Hosung Choo[1]

[1] School of Electronic and Electrical Engineering, Hongik University, Seoul, Korea; Corresponding author: hschoo@hongik.ac.kr

[2] Department of Electronics and Computer Engineering, Hanyang University, Seoul, Korea

Received 19 May 2015

ABSTRACT: *This article proposes the design of microstrip patch antennas to improve low-elevation gain for controlled reception pattern antenna (CRPA) applications. The proposed antenna consists of a main resonant patch and a subpatch that are electromagnetically coupled with each other to operate as a two-element array whose bore-sight direction points toward low-elevation angles. The array factor is then enhanced by inserting a ceramic substrate with a high dielectric constant to maximize the electrical distance between the patches. As a result, the average gain at $\theta = 75°$ is enhanced by 1.2 dB, which demonstrates that the proposed antenna is suitable to be used for the individual elements of CRPA arrays with the improved radiation gain at low-elevation angles.* © 2016 Wiley Periodicals, Inc. Microwave Opt Technol Lett 58:170–174, 2016; View this article online at wileyonlinelibrary.com. DOI 10.1002/mop.29517

Key words: *global positioning system antenna; controlled reception pattern antenna array antenna; microstrip patch antennas*

1. INTRODUCTION

Controlled reception pattern antenna (CRPA) arrays have been proposed to mitigate the effects of interferences in the global positioning system by steering nulls toward interference sources. For more successful null steering operation, the individual elements of CRPA arrays should have circular polarization (CP), uniform pattern, and high gain, especially at low-elevation angles [1]. The low-elevation gain is important for CRPA arrays because the array simultaneously receives satellite signals during the null steering operation that often takes place at low-elevation angles [2,3]. Although, this low-elevation gain is one of the key design considerations of CRPA arrays, most of the previous studies focused on improving the bore-sight gain [4] and CP properties by adopting asymmetric structures [4–8] and external chip couplers [9,10]. Thus, more sophisticated research has been required to improve low-elevation gain for enhanced CRPA performance.

In this article, we propose a design of a microstrip patch antenna that enhances the low-elevation gain for CRPA applications. The low-elevation gain is improved by inserting an additional subpatch above a main patch that is fed by a coaxial cable. The subpatch is then electromagnetically coupled to the main patch, which allows the antenna to operate as a two-element array. The array factor is further enhanced by inserting a ceramic substrate with a high dielectric constant between the two patches to increase their electrical distance. To demonstrate the suitability of the proposed antenna, it is fabricated and its antenna characteristics, such as reflection coefficients, gains, patterns, and axial ratio (AR), are measured in a full anechoic chamber. The results prove that the proposed antenna is suitable for an individual element of CRPA arrays with the enhanced low-elevation gain.

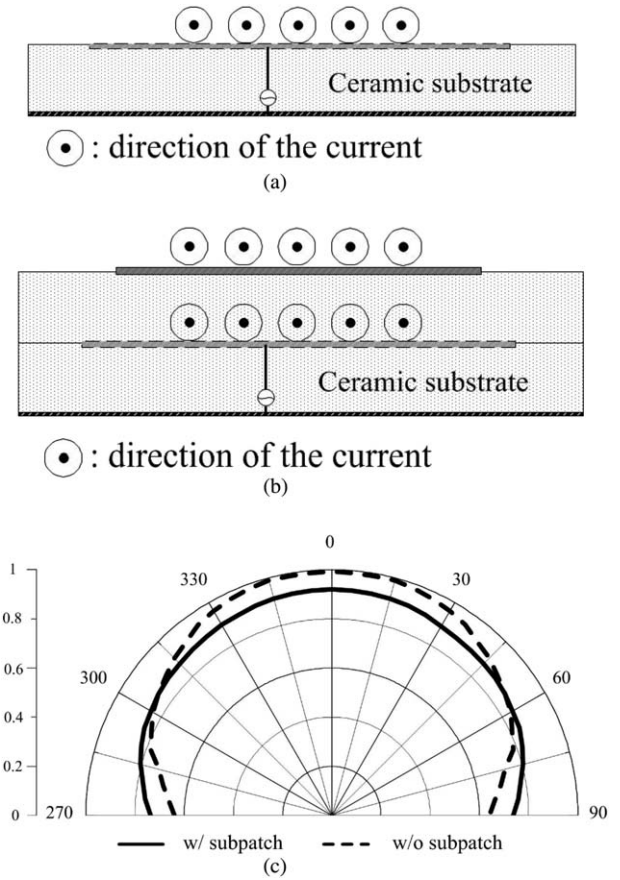

Figure 1 Design approach using the subpatch (a) current distribution without the subpatch, (b) current distribution with the subpatch, and (c) pattern enhancement at low-elevation angles

2. DESIGN APPROACH AND PROPOSED ANTENNA

Figure 1 shows our design approach for enhancing the radiation gain at low-elevation angles, which is an important design consideration for individual elements of CRPA arrays. The conventional microstrip patch antenna, illustrated in Figure 1(a), has a maximum directivity at $\theta = 0°$ and is less directive in the azimuth direction ($\theta = 90°$) due to its low-profile characteristics. Thus, we insert an additional patch above the existing patch to use an array factor in the azimuth direction for increased directivity at low-elevation angles, as shown in Figure 1(b). In our design, the two patches are electromagnetically coupled with each other to induce currents on the upper patch and operate as a two-element array so that the broad-side direction of their array factor lies in the azimuth plane. To maximize the directive gain of our design at low-elevation angles, the current density of the upper patch should be maintained as high as the lower patch, and the phase difference of the induced currents between the two patches should be minimized. For further improvement, we place a high dielectric ceramic substrate between the two patches to increase their electrical distance by about a square root of the dielectric constant. Figure 1(c) shows a comparison of radiation patterns in the *E*-plane, which explains that the gain of the proposed antenna structure can be improved at low-elevation angles by the additional patch.

Figure 2 illustrates the geometry of the proposed antenna structure, which consists of a main patch and a subpatch. The edge length of the main patch is w_2, which is designed to be

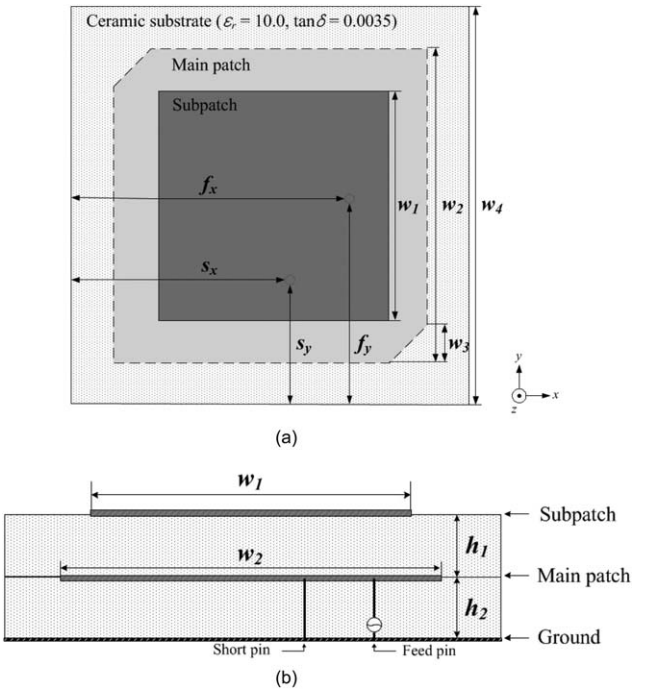

Figure 2 Geometry of the proposed antenna (a) top view and (b) side view

TABLE 1 Optimized Values of the Proposed Antenna

Parameters	Value
w_1	25.9 mm
w_2	26.6 mm
w_3	4.9 mm
w_4	50.0 mm
f_x	34.7 mm
f_y	25 mm
s_x	24.4 mm
s_y	19.0 mm
h_1	3.14 mm
h_2	6.28 mm

approximately a half wavelength in the L1 band, and the patch is printed on a ceramic substrate (CER10 from Taconic, $\varepsilon_r = 10.0$, tan $\delta = 0.0035$) with a thickness of h_2 and an edge

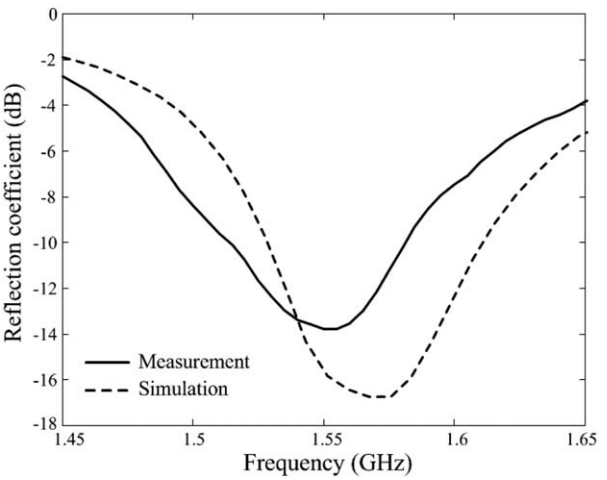

Figure 3 Reflection coefficients of the proposed antenna

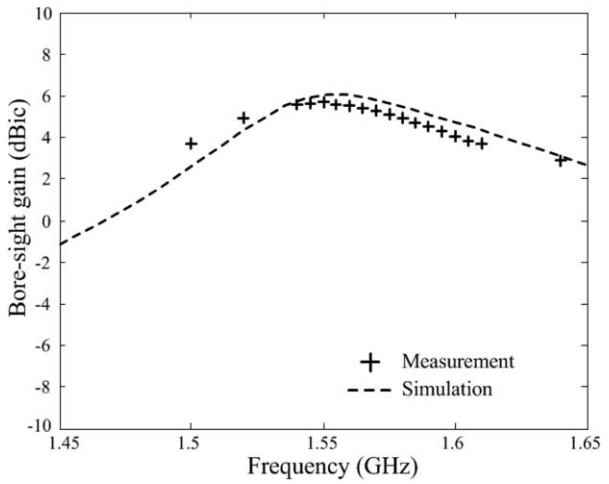

Figure 4 Bore-sight gain of the proposed antenna

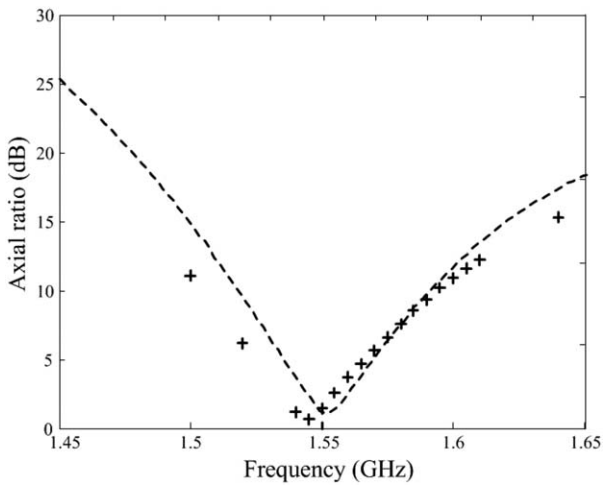

Figure 5 AR of the proposed antenna

length of w_4. The patch is fed by a coaxial probe, denoted as a feed pin, and the feeding position is determined with f_x and f_y. The two corners of the patch are truncated by w_3 to obtain CP characteristics, and the CP bandwidth is improved by connecting

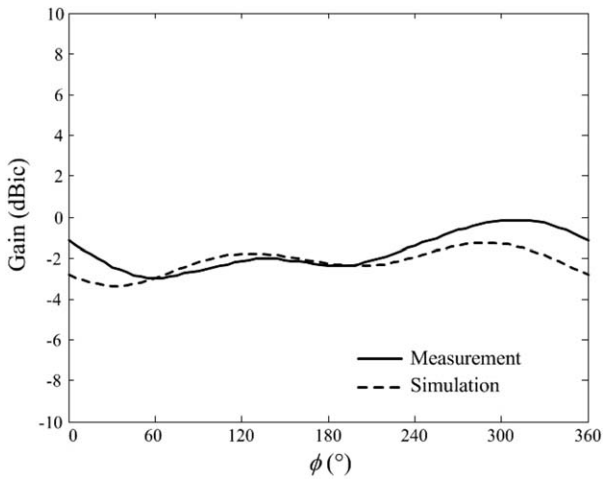

Figure 6 Radiation gain at $\theta = 75°$

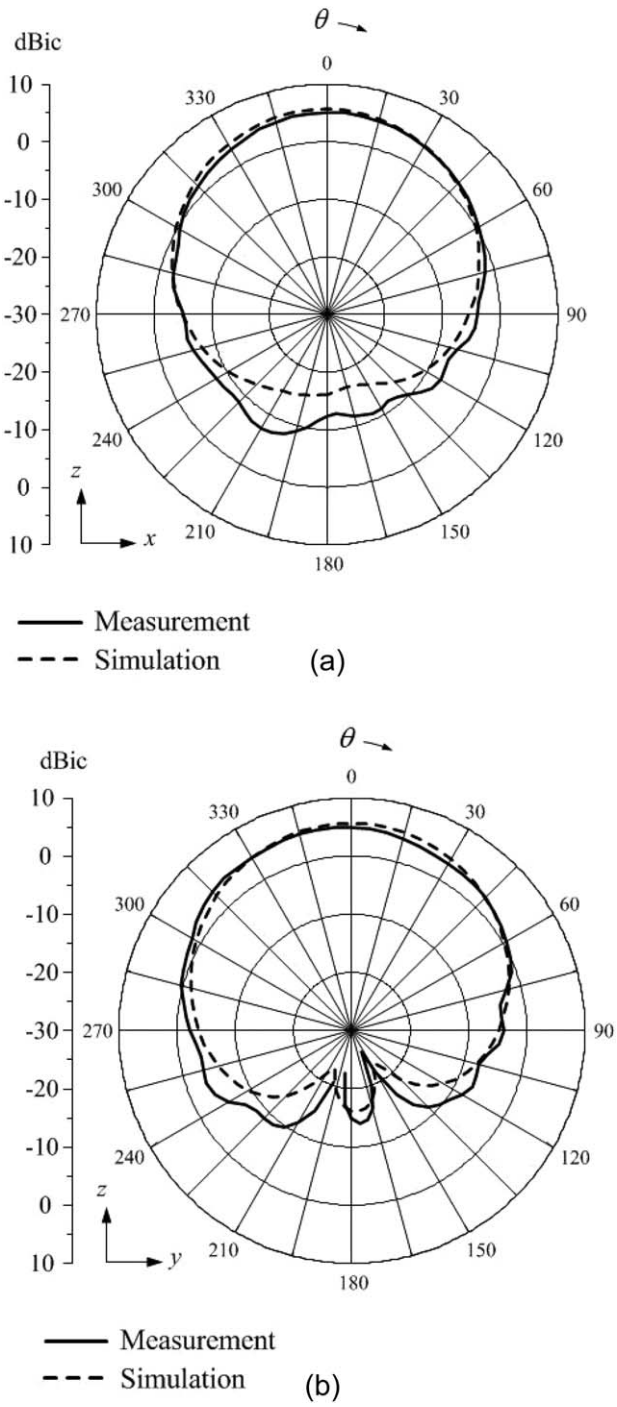

Figure 7 Two-dimensional patterns of the proposed antenna (a) *zx*-plane and (b) *zy*-plane

the patch to the ground via a short pin expressed by s_x and s_y. Then, the subpatch is designed to be electromagnetically coupled with the main patch for inducing currents in the same direction as the main patch, and the coupling strength is adjusted by the width of the subpatch (w_1) and the thickness of the upper substrate (h_1).

To further improve the antenna performances, the proposed antenna structure is optimized by a genetic algorithm [11] in conjunction with the FEKO EM simulator [12], and the final dimensions are shown in Table 1. As expected, the optimized edge length of the main patch is about a half of the effective wavelength, and the subpatch is optimized to be slightly smaller

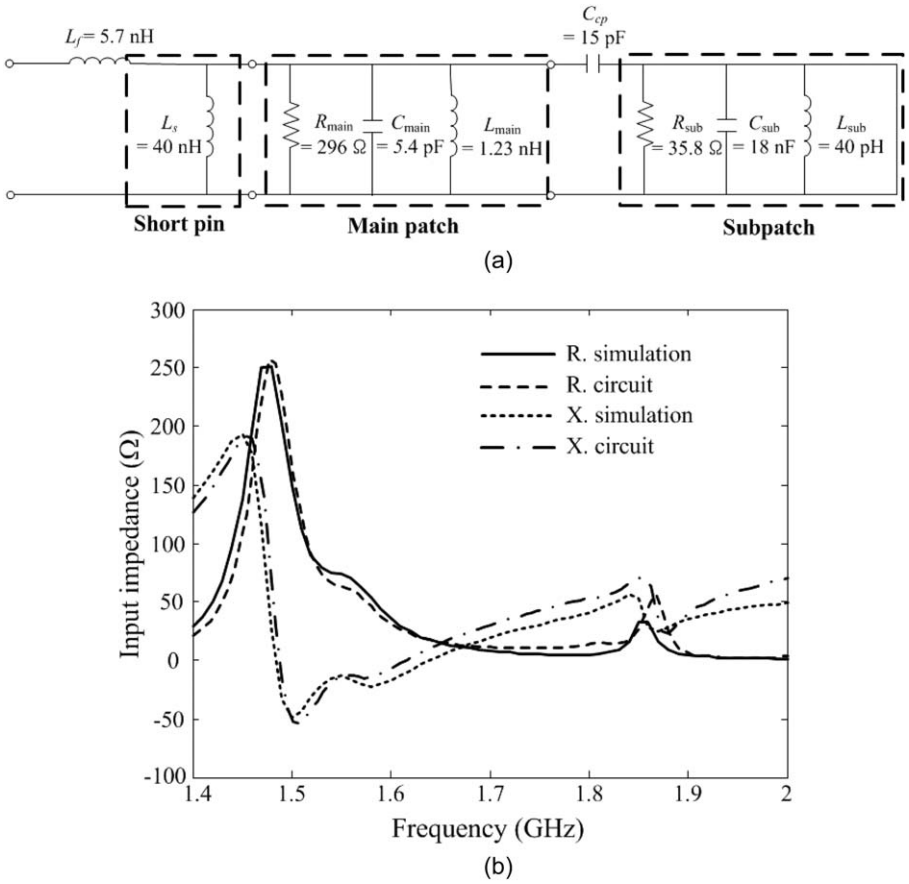

Figure 8 Equivalent circuit model (a) circuit model and (b) input impedance

than the main patch. For electromagnetic coupling, the subpatch is placed close to the main patch to induce high-density currents with the same phase.

3. MEASUREMENT AND ANALYSIS

To verify the antenna characteristics, such as reflection coefficients, gains, patterns, and AR, the proposed antenna is fabricated and mounted at the center of a circular ground platform with a diameter of 140 mm. Figure 3 shows a comparison of the reflection coefficients between the simulation and the measurement, which are represented by dashed and solid lines, respectively. The measured reflection coefficient of the antenna is -11.2 dB at 1575 MHz, and the 10-dB matching bandwidth is 65 MHz ($|S_{11}| < -10$ dB, 1515–1580 MHz). Figure 4 exhibits the measured bore-sight gain compared with the simulation. The simulated data are presented by a dashed line and the measured data are specified by "+" marks. Both results show good agreement with the peak values of 5.1 dBic for the measurement and 5.7 dBic for the simulation. Figure 5 illustrates the AR as a function of the frequency, which is provided to demonstrate the CP characteristics of the antenna. The antenna shows the minimum AR of 0.69 dB at 1545 MHz with a 3-dB AR bandwidth from 1535 to 1555 MHz, which is similar to the simulated value of 20 MHz from 1542 to 1562 MHz.

Figure 6 represents radiation patterns in the azimuth direction at $\theta = 75°$. The proposed antenna shows an average gain of -1.7 dBic with a minimum value of -2.9 dBic, and the pattern is uniform with a gain deviation of less than 2.9 dB. Figures 7(a) and 7(b) show measured radiation patterns at 1575 MHz that are compared with the simulation. The antenna exhibits a half-power beamwidth (HPBW) of 160° in the *zx*-plane and 170° in the *zy*-plane, which agrees well with the simulation whose HPBWs are 155° and 165°, respectively. The results demonstrate that the improved low-elevation gain also results in broad HPBWs of greater than 100° without any serious pattern distortions.

To interpret the operating principle of the proposed antenna from the circuit point of view, an equivalent circuit model is built by a data-fitting method, and each component of the antenna, such as the feed pin, the short pin, the main patch, and the subpatch, is specified in the circuit. The circuit and its detailed parameters are shown in Figure 8(a), and the input impedance of the circuit is illustrated in Figure 8(b) in comparison with that of the EM simulation. The antenna has an input resistance of about 50 Ω at the resonant frequency, and its reactance value is close to 0 Ω for both results. In addition, a small fluctuation around the resonant frequency is caused by the short pin, which broadens the matching bandwidth due to the reduced slope of the reactance curve.

To analyze the gain enhancement at low-elevation angles, the amplitude, and the phase of the induced current density on the two patches are observed, as illustrated in Figure 9(a). The amplitude and phase information of the main patch are specified by circles, and those of the subpatch are marked with rectangles. The current amplitudes of the two patches are 15.5 and 8.0 A/m at 1575 MHz, and their phase difference is less than 5°, which results in increased directivity of 1.2 dB at low-elevation angle ($\theta = 75°$), as shown in Figure 9(b). The curve is calculated as the gain enhancement $\theta = 75°$ of the proposed antenna compared with the conventional antenna structure, which demonstrates that our design approach is capable of improving the low-elevation gain.

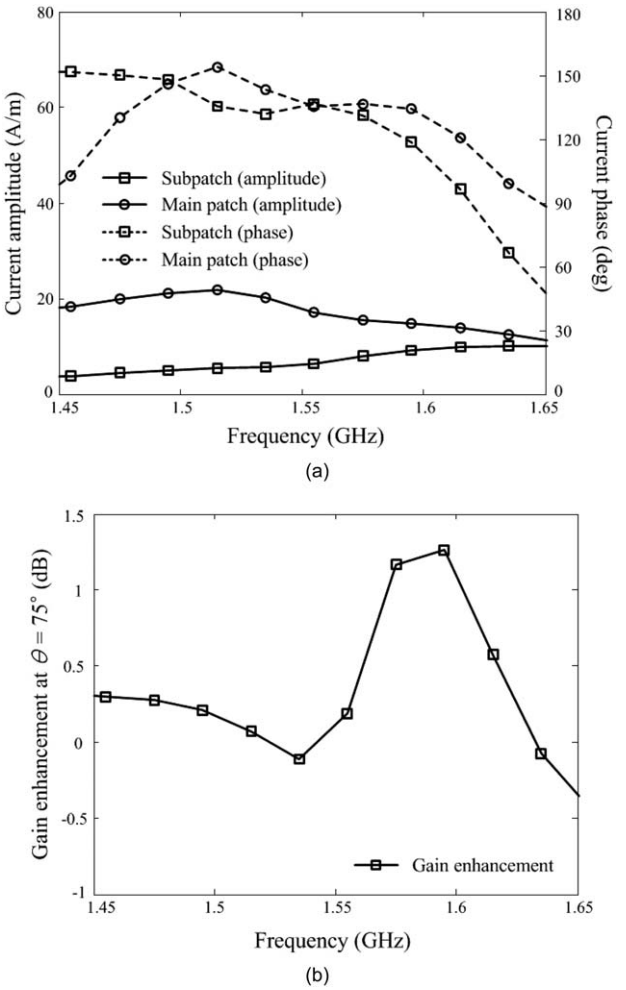

Figure 9 Analysis of gain enhancement at low-elevation angles (a) amplitude and phase of the induced current and (b) gain enhancement at $\theta = 75°$

4. CONCLUSION

We investigated the design of a microstrip patch antenna with improved low-elevation gain for CRPA applications. The proposed antenna is composed of the main patch and a subpatch, and the two patches were designed to be electromagnetically coupled for the same direction current by adjusting the size of the subpatch and the substrate height. The proposed antenna was fabricated and mounted on a 140-mm circular ground platform to measure its antenna characteristics. The measured reflection coefficient was −11.2 dB at 1575 MHz with a bore-sight gain of 5.1 dBic, and the average gain at $\theta = 75°$ was −1.7 dBic with an average HPBW of 165°. The results proved that the proposed antenna is suitable to enhance the low-elevation gain and can be used as the individual element of CRPA arrays.

ACKNOWLEDGMENTS

This research was supported by Civil Military Technology Cooperation (CMTC) and the Basic Science Research Program through the National Research Foundation of Korea (NRF) funded by the Ministry of Education (NRF-2014R1A1A2055813).

REFERENCES

1. J.R. Lambert, C.A. Balanis, and D. DeCarlo, Spherical cap adaptive antennas for GPS, IEEE Antennas Propag Mag 57 (2009), 406–413.
2. P. Enge, T. Walter, S. Pullen, C. Kee, Y.C. Chao, and Y.J. Tsai, Wide area augmentation of the global positioning system, IEEE Proc Mag 84 (1996), 1063–1088.
3. S. Datta-Barua, J. Lee, S. Pullen, M. Luo, A. Ene, D. Qiu, G. Zhang, and P. Enge, Ionospheric threat parameterization for local area global-positioning-system-based aircraft landing systems, J Air 47 (2010), 1141–1151.
4. F.S. Chang, K.L. Wong, and T.W. Chiou, Low-cost broadband circularly polarized patch antenna, IEEE Antennas Propag Mag 51 (2003), 3006–3009.
5. T.N. Chang and J.M. Lin, Circularly polarized antenna having two linked slot-rings, IEEE Antennas Propag Mag 59 (2011), 3057–3060.
6. K.L. Wong and Y.F. Lin, Circularly polarised microstrip antenna with a tuning stub, IEEE Electron Lett 34 (1998), 831–832.
7. H.M. Chen and K.L. Wong, On the circular polarization operation of annular-ring microstrip patch antennas, IEEE Antennas Propag Mag 47 (1999), 1289–1292.
8. W.S. Chen, C.K. Wu, and K.L. Wong, Single-feed square-ring microstrip antenna with truncated corners for compact circular polarisation operation, Electron Lett 34 (1998), 1045–1047.
9. G. Byun, S. Kim, and H. Choo, Design of a dual-band GPS antenna using a coupled feeding structure for high isolation in a small array, Microwave Opt Technol Lett 56 (2014), 359–361.
10. G. Byun, S.M. Seo, I. Park, and H. Choo, Design of small CRPA arrays for dual-band GPS applications, IEICE Trans Commun E97B (2014), 1130–1138.
11. Y. Rahmat-samii and E. Michielssen, Electromagnetic optimization by genetic algorithms, Wiley, New York, 1999.
12. FEKO Suite 7.0, EM software and systems, Available at: http://www.feko.info, 2014.

8-ANTENNA AND 16-ANTENNA ARRAYS USING THE QUAD-ANTENNA LINEAR ARRAY AS A BUILDING BLOCK FOR THE 3.5-GHz LTE MIMO OPERATION IN THE SMARTPHONE

Kin-Lu Wong,[1] Jun-Yu Lu,[1] Li-Yu Chen,[1] Wei-Yu Li,[2] and Yong-Ling Ban[3]
[1] Department of Electrical Engineering, National Sun Yat-Sen University, Kaohsiung 80424, Taiwan; Corresponding author: wongkl@ema.ee.nsysu.edu.tw
[2] Information and Communications Research Laboratories, Industrial Technology Research Institute, Hsinchu 31040, Taiwan
[3] Institute of Electromagnetics and School of Electrical Engineering, University of Electronic Science and Technology of China, Chengdu 611731, China

Received 19 May 2015

ABSTRACT: *Using the quad-antenna linear (QAL) array as a building block, the 8-antenna and 16-antenna arrays for the 3.5-GHz long term evolution multiple-input multiple-output (MIMO) operation in the smartphone are demonstrated. The QAL array has a planar structure of narrow width 3 mm (0.035λ) and short length 50 mm (0.58λ), with λ being the wavelength at 3.5 GHz. For the 8-antenna array, two QAL arrays are disposed along two opposite side edges (denoted as Array A) or the same side edge (denoted as Array B) of the system circuit board of the smartphone. The obtained envelope correlation coefficient values of the antennas in Array A and B are shown. The calculated channel capacities for Array A and B applied in an 8 × 8 MIMO system are also analyzed. The 16-antenna array formed by four QAL arrays disposed along two opposite side edges (denoted as Array C) is then studied. For operating in a 16 × 16 MIMO system, the calculated channel capacity of Array C can reach about 66–70 bps/Hz with a 20-dB signal-to-noise ratio. The obtained channel capacity is about 5.7–6.1 times that (11.5 bps/Hz) of the upper limit of an ideal 2 × 2 MIMO system with 100% antenna efficiency for*